
Article:
Duraman, SB and Richardson, IG (2020) Microstructure & properties of steel-reinforced concrete incorporating Portland cement and ground granulated blast furnace slag hydrated at 20 °C. Cement and Concrete Research, 137. 106193. p. 106193. ISSN 0008-8846

https://doi.org/10.1016/j.cemconres.2020.106193

Microstructure & Properties of Steel-Reinforced Concrete Incorporating Portland Cement and Ground Granulated Blast Furnace Slag Hydrated at 20°C

Saiful Baharin Duraman[a,b,*] & Ian G. Richardson[a,]**

[a] School of Civil Engineering, University of Leeds, Leeds, LS2 9JT, United Kingdom

[b] Faculty of Engineering, Universiti Teknologi Brunei, BE 1410, Brunei Darussalam

[*]Corresponding Author; Tel: +673 2461020; E-mail: saiful.duraman@utb.edu.bn

[**]Tel: +44 113 343 2331; E-mail: i.g.richardson@leeds.ac.uk

Abstract

The results of a backscattered electron imaging study of the microstructure of the steel- and aggregate-cement paste interfaces of reinforced concrete systems hydrated at 20 ℃ temperature are reported. The mix using neat OPC showed increasing calcium hydroxide (CH), and decreasing porosity and anhydrous cement levels with respect to age. Higher CH and porosity, and lower anhydrous cement levels at the interfaces compared to the bulk cement were also shown. Mixes incorporating ground granulated blast furnace slag (GGBS) at various cement replacement levels showed consistently low CH, and decreasing porosity, anhydrous cement and unreacted slag levels with respect to age. Higher CH and porosity, and lower anhydrous cement and unreacted slag at the interfaces compared to the bulk were also shown. The slope profiles of unreacted slag at the interfaces were steeper suggesting a narrower interfacial transition zone and thus tighter packing for the GGBS incorporated mixes.

Keywords: Backscattered Electron Imaging (B); Image Analysis (B); Interfacial Transition Zone (B); Characterisation (B); Granulated Blast-Furnace Slag (D)

1. Introduction

The most common cause of durability loss in steel reinforced concrete is corrosion of the steel reinforcement bars, or more commonly called steel rebars. This is of great socio-economic importance, with direct losses (e.g. rehabilitation, repair and maintenance) in the range of billions of US dollars per annum worldwide [1]. An area of interest with respect to reinforced concrete is the 'lime layer hypothesis'. The initial assumption was that the interface region between the steel rebar and the concrete is composed of largely segregated lime (calcium hydroxide) (CH) from the hydration reaction of the calcium silicates, and ensures the passive state of the steel rebar (e.g. [2-4]). Many of these earlier studies on the steel-concrete interfaces however used fractured surfaces which may preferentially occur at weaker areas.

The use of backscattered electron (BSE) imaging of polished sectioned specimens is becoming widespread in concrete microstructural studies, partly because when combined with the process of image analysis, it provides a method of obtaining quantitative results that are unbiased and therefore more representative of the concrete system. The difficulties of obtaining representative specimens and the rigorous specimen preparation process may be a possible reason why there have been few studies made on the steel-concrete interfaces using polished cut sections (e.g. [5-9]). There are even fewer studies quantitatively characterising the distribution of hydration products from the steel-concrete interfaces (e.g. [6-9]); this may be attributed to the time-consuming factor of the image analysis process [10].

Based on qualitative observations of BSE micrographs, Glass et al. [5] concluded that there was no preferential arrangement of hydration products at the steel-concrete interface. Due to difficulties in specimen preparation, 200 μm steel ribbons were used to emulate steel rebars. It is likely that this small size may have contributed to the finding since the physical interaction of the ribbon during the

53 placing and compacting stages may have led to non-preferential arrangement of the concrete
54 components and cement hydration products. If a typical cement particle size is taken as 20 μm, then
55 the ribbon, which would be acting as a "wall", would be 10x larger than that cement particle.
56 However, a rebar of 8 mm diameter would be 400x larger than that same cement particle. Zayed [6]
57 performed quantitative analysis of BSE micrographs and found no increases of CH at the interfaces.
58 However, it is likely that the image selection may have included undersides of rebars, which would
59 have different profiles than the topsides (as discussed later in Section 3.1. Qualitative Microstructural
60 Observations). The width of the strips used in the image analysis process may have also been too
61 wide (as discussed later in Section 2.5. Image Analysis). Horne et al. [7] performed quantitative
62 analysis of BSE micrographs, and classified images in accordance with the orientation of the rebars;
63 and also between top and underside of the rebar ribs. They concluded that the top of the ribs of
64 rebars cast in vertical direction and topside of rebars cast in horizontal direction had higher amounts
65 of CH at the interface as compared to the bulk cement paste.
66
67 Incorporation of cement replacements including Ground Granulated Blast Furnace Slag (GGBS) into
68 concrete may satisfy intended properties such as improved durability, as well as contributing towards
69 environmental sustainability. Many studies (e.g. [11-15]) confirm the superiority of GGBS
70 incorporated concrete as compared to plain concrete systems. Mohammed et al. [15] compared the
71 interfaces of reinforced concrete systems and based on qualitative secondary electron imaging (SEI)
72 observations and electron microprobe analyser tests concluded that concrete incorporating GGBS
73 had a denser C-S-H morphology than neat ordinary Portland cement (OPC) concrete, and that the
74 denser morphology blocked chlorides from penetrating into the system. This conclusion of denser C-
75 S-H morphology is consistent with the different morphology of C-S-H in slag-rich cement blends when
76 compared with neat OPC, as observed by Richardson & Groves [16] and Taylor et al. [17] using
77 transmission electron microscopy (TEM).
78

Whilst few quantitative studies utilising BSE micrographs have been reported on reinforced concrete systems as discussed previously, there does not appear to be any for concrete systems incorporating GGBS. This may likely be due to difficulties of specimen preparation as discussed previously (and also later in Section 2. Experimental Methodology), and also due to difficulties in allocation of the hydration products (as discussed later in Section 2.5. Image Analysis). This article reports findings of comparison studies done for steel reinforced concrete systems incorporating neat OPC and OPC/GGBS, including the qualitative and quantitative microstructural findings of the properties at the steel- and aggregate-cement interfaces.

2. Experimental Methodology

2.1. Materials & Moulds Used

The main binder used was ordinary Portland cement which also conforms to BS EN 197 Portland Cement CEM 1 classification, with mineral composition approximately 50.4% C_3S, 22.2% C_2S, 8.4% C_3A and 9.2% C_4AF, and henceforth referred as OPC. Ground Granulated Blastfurnace Slag (GGBS) was also used as partial cement replacement. Binder information for the OPC and GGBS including oxide composition and typical specific surface area (SSA) is summarised in **Table 1**. The coarse aggregates (CA) and fine aggregates (FA) used were of quartzitic nature and of gravel type and obtained from the same quarry. The physical properties of the CA was a blend of crushed and uncrushed type and of 10mm nominal maximum size; this size was preferred due to the microstructural nature of the study. The aggregates were segmentable in the Image Analysis process, utilising elemental distribution maps as per Brough & Atkinson [18]. Water used was clean and potable water to simulate on-site conditions.

Table 1 – Binder Information for OPC and GGBS Used In Study

Chemical Constituent %	SiO_2	Al_2O_3	Fe_2O_3	CaO	MgO	Na_2O	K_2O	TiO_2	SO_3

OPC	21.15	5.13	3.04	64.51	2.15	0.27	0.58	-	2.67
GGBS	34.45	13.21	0.60	38.07	8.06	<0.30	0.41	0.49	-

The reinforcement used was 8mm plain (i.e. non-ribbed) 250Y grade mild steel reinforcement bars. These were preferred due to ability to be analysed in both vertical and horizontal orientation, and were the most optimum with respect to the specimen preparation methodology utilised. Non-ribbed rebars were also preferred as Horne et al. [7] had used ribbed rebars and found differences in properties of concrete microstructure at the top and underside of rebar ribs for concrete cast in vertical direction. The rebars were purposely left as-is, with only loose rust removed, to simulate on-site conditions. Moulds used were 150mm cube moulds purposely constructed for the study. Different moulds were used which ensured fixed alignment of the steel rebars in either vertical or horizontal directions, emulating fixed on-site conditions. The rebars were positioned rigidly in the final location prior to casting of the concrete, as per on-site conditions, and therefore addressed the possible ambiguity on whether the rebars were positioned prior or after the concrete had been placed. Whilst practices had been undertaken to simulate on-site conditions as much as possible in-lab, it is appreciated that other real on-site factors may also have effect on the results, for example rust on rebars, intersection of rebars, presence of tie-wires or contamination of rebar surface [19]. These are however isolated and/or controlled for this study to reduce the possibility of results being affected by unknown factors.

2.2. Summary of Concrete Mixes

This article discusses the results from 3 principal concrete mixes. These comprise of GGBS used as cement replacement at 0% (i.e. a neat OPC concrete mix), 50% and 70% replacement levels and referred as OPC Mix, 50GGBS Mix and 70GGBS Mix respectively. The mixes were cured at 20°C temperature at 100% humidity conditions. Specimens were then obtained via coring at various ages including 1, 3, 7, 28 and 270 days. It was not possible to obtain 1 day age specimens from the GGBS

mixes since the concrete had not hydrated and hardened enough to withstand the coring process. A series of tests were done for each mix, which included tests for fresh and hardened properties, and microstructure tests. The scope of work also included similar concrete (and cement) mixes produced and cured at simulated elevated temperature conditions. This article concentrates on microstructural analysis of the mixes cured at 20°C whereas the results for those cured at elevated temperature will be published elsewhere. The mean compressive strength results of the mixes, as summarised in **Table 2**, will be compared later with the findings from the microstructural study.

Table 2 – Mean compressive strength results

Mix	Mean Compressive Strength (MPa) at Age				
	1 Day	3 Day	7 Day	28 Day	270 Day
OPC Mix	14.60	30.35	43.70	59.70	76.80
50GGBS Mix	8.05	19.65	30.15	50.65	80.20
70GGBS Mix	4.35	11.40	22.31	43.00	66.60

To take into consideration the potential variability property of concrete, the experiments were devised such that all results were from the same mixes. In addition, the materials for the concrete mixes were all from the same batch to further reduce potential discrepancies due to materials properties. A default mix design of CA:FA:binder ratio by weight of 3:2:1 and a water/binder ratio by weight of 0.5 was utilised for the mixes. Cement replacement used was percentage replacement by weight.

Based on results of trial mixes, the selected default water/binder ratio of 0.5 was found to be optimal. Concrete consistence (or formerly referred as concrete workability) could be measured using a single indirect consistence test, in this case the Slump Test, and therefore direct comparisons of concrete consistence could be made between all mixes. Full compaction was achieved for all mixes at this water/binder ratio; avoiding inadequate compaction for the mix with the lowest consistence and ensuring cohesiveness remained for the mix with the highest consistence. The mixes were

compacted using a mechanical vibrating table, with compaction ensured once all the air bubbles from the fresh concrete were eliminated, and immediately stopped before segregation occurred. The water/binder ratio used did not necessitate using chemical admixtures, which may have otherwise compromised the findings, especially due to the microstructural nature of the study.

2.3. Specimen Preparation

At the required age, reinforced concrete of approximately 25mm in diameter with the rebar in the centre, was cored using a water-cooled concrete core drill equipped with a diamond-bit core barrel. Specimens with the steel-concrete interfaces exposed were then obtained by cutting through the specimens either through the vertical (longitudinal) axis of the cores for rebars of vertical orientation, or through the horizontal (transversal) axis of the cores for rebars of horizontal orientation, using a water-cooled concrete cutting saw (Discoplan-TS Streurs). The blade was diamond-tipped and able to cut through both concrete and steel rebar. Hydration was stopped by immersion of the specimens in liquid nitrogen and then freeze dried using a freeze drier, thus allowing analysis to be done at later ages.

Preliminary grinding was initially performed to eliminate defects due to the original cutting process and expose the real specimen surface behind the cut surface. This was achieved by manually grinding each specimen using coarser sized silicon carbide abrasive paper. A reflected light microscope (Ziess) was used to visually assess the specimen quality. Each specimen was then epoxy impregnated to preserve its features during the subsequent grinding and polishing stage.

The grinding and polishing process was done using a grinding and polishing machine (Struers Rotopol) equipped with a rotating turntable. Silicon carbide papers of successively finer sizes placed on the machine were used to grind and polish the specimen until it was flat enough for

178 microstructural analysis via BSE imaging using a scanning electron microscope (SEM). A reflected light
179 microscope was similarly used to assess the specimen quality and whether it was acceptable to
180 proceed to the subsequent grinding/ polishing stage using finer-sized paper. In general, a specimen
181 was considered acceptable to proceed to the next grinding/ polishing stage once most of the defects
182 from the previous grinding/ polishing stage has been predominantly eliminated. The specimen face
183 to be analysed was then sputter coated with a thin film of carbon. It is noted that the grinding and
184 polishing process was one of the difficult parts of the specimen preparation stage partly because of
185 the difficulty of preparing reinforced concrete specimens representative of the system and the
186 importance of user experience, and has major effect on the quality of the specimen to be analysed.
187
188
189 **2.4. Microstructural Analysis**
190 The principal investigation was quantification of the distribution of hydration products from both the
191 steel- and aggregate-cement interfaces using image analysis of the BSE micrographs and elemental
192 distribution maps of areas of the specimens. A CamScan Series 4 SEM was used to examine the
193 specimen. The SEM was equipped with an energy dispersive X-ray (EDX) detector (Oxford
194 Instruments EDX) which was used to collect elemental maps and quantitative analyses of selected
195 points. Optimum settings used for BSE imaging (and also EDX mapping) was an accelerating voltage
196 of 20 keV, a spot size of 1, a working distance of 28 mm and a tilt angle of 0°. The settings were
197 optimum with respect to factors including resolution, specimen damage, aberration and perspective.
198
199 The specimen was initially viewed in SEI mode. This allowed the user to confirm the flatness of the
200 area to be analysed and also allowed less bias of preferential acquisition of specific features (e.g.
201 selecting areas of high CH content) since the user was less aware of the hydration product
202 distribution of that area. Micrographs in BSE imaging mode were then taken of random areas which
203 contained the distribution of hydration products at the steel-cement interface. These areas also

204 generally showed the aggregate-cement interface. Damaged areas (such as cracking) and air voids
205 not part of the microstructure were avoided. For each area, X-ray maps of specific elements were
206 also recorded.
207
208
209 **2.5. Image Analysis**
210 An image analysis software (KS400 Imaging System Software, Carl Zeiss Vision GmbH) was used to
211 extract quantitative information from each set of BSE micrographs and the elemental maps taken.
212 Binary masks were produced by allocating a specific range within the greyscale histograms for phases
213 which have clear allocations, or from a single or a combination of specific elemental distribution
214 maps. The former method was preferred since the elemental maps were of lower quality than the
215 BSE micrographs, but in situations of greyscale level overlaps, the latter was more optimal.
216
217 Porosity maps (for pores with width greater than about 0.5 μm), CH maps, anhydrous cement maps,
218 aggregate maps and steel maps were obtained as per method utilised by Horne et al. [7] (and
219 outlined by Richardson [20]). In addition, CH maps could also be formed from the arithmetic
220 production of the calcium (Ca) and silicon (Si) elemental maps. These were necessary for the GGBS
221 mixes since the unreacted slag particles were at similar greyscale levels with the CH. For the GGBS
222 mixes, unreacted slag binary masks were therefore obtained from the arithmetic subtraction of the
223 CH binary mask from the combined CH & GGBS binary mask (which were at similar greyscale levels).
224 The remaining binary mask was for the C-S-H; this was obtained by the total area subtracted with the
225 sum of the other binary masks, including the steel and aggregate. Due to known inclusions and/or
226 intermixing of CH, monosulphates, ettringite and pores which are too fine to be distinguished at the
227 magnification level used, these are termed as undesignated hydration products (UHP).
228

229 Successive strips were then produced from the steel-cement interface to the bulk cement paste,
230 each strip being 4 pixels in width which equates to approximately 1.88 μm. The width used was
231 similar to Horne et al. [7] and was found to be optimal in terms of avoiding local variation or intrinsic
232 heterogeneity [10] if too narrow, and unrepresentative average if too wide. As a comparison, Zayed
233 [6] used strip width of approximately 5 μm which may have considerably averaged the results
234 obtained. 50 strips, equating to 94 μm total width were produced; it is considered that this would be
235 bulk cement. The width utilised is based on Horne et al. [7] who used total width of approximately
236 120 μm for both the steel- and aggregate-cement interfaces, and Scrivener [21] who considered that
237 the most significant differences in properties occurs over the first 15-20 μm from the interface with
238 respect to the aggregate-cement interfacial transition zone (ITZ).
239
240 The distribution of hydration products in each strip was then recorded. Similar strips were produced
241 from the aggregate-cement paste interface, with consideration given so that both the strips from the
242 steel-cement and aggregate-cement interfaces did not overlap with one another, thus avoiding
243 duplicate results. This process meant that the total area of the strips reduced towards the bulk
244 cement paste from each interface, and so this reduced accuracy towards the bulk should therefore
245 be considered. Horne et al. [7] illustrated the reducing accuracy whereby the 95% confidence
246 intervals became larger due to the number of images contributing to the result decreasing as the
247 distance from the interface increases. The number of images utilised was up to 60 images from 2
248 specimens. Duraman [22] similarly showed a graphical example via a specimen where the total
249 cumulative area at the steel-concrete interface was 42000 pixels which reduced to 20000 pixels at
250 the furthest point from the interface. **Figure 1** demonstrates the production of strips from the steel-
251 and aggregate-cement interfaces based on the original BSE micrograph using image analysis.
252

Figure 1- BSE micrographs at 500× magnification showing (a) the original image and (b) the production of strips from the steel- and aggregate-cement interfaces via image analysis.

The distribution of hydration products in each strip was subsequently recorded.

(a) (b)

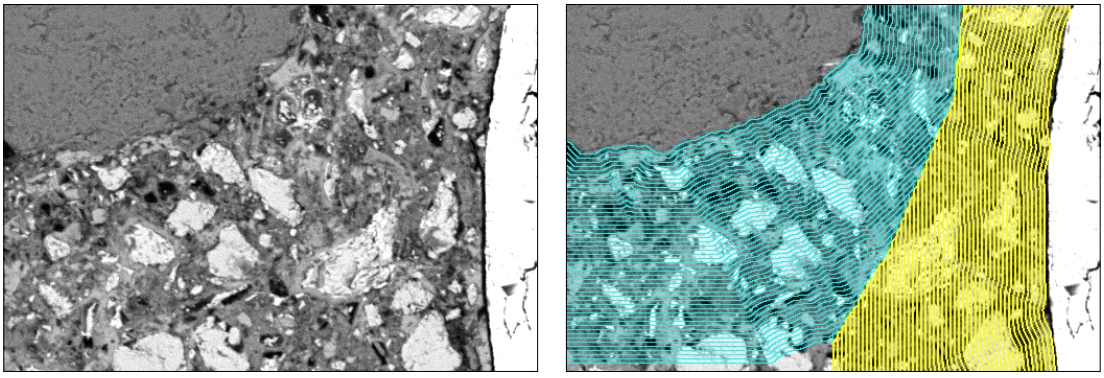

Macro functions within the image analysis software were developed for the above processes due to the repetitive nature. Specific sets of macros were developed for each concrete system. For each mix at each age, up to 60 sets of images were taken from 2 to 3 specimens. This number was similar to Horne et al [7] who concluded that this was the highest practicable number possible within reasonable timescales to provide statistically significant profiles, in addition to reduced accuracy towards the bulk. Scrivener [10, 21] had previously acknowledged the time factor to be one of the biggest obstacles of quantitative characterisation of BSE images.

3. Results and Discussion

3.1. Qualitative Microstructural Observations

The 'wall-effect' with the steel rebar acting as the wall was observed at lower magnification levels (e.g. **Figure 2** at 50x magnification) with larger sized aggregates (not necessarily CA) predominantly a considerable distance away from the steel interface. Likewise the wall-effect with the CA acting as a wall was also observed with no CA being in close vicinity with other CA and agrees with qualitative observation from other studies (e.g. [23, 24]). **Figure 2** and **Figure 3** shows examples of regular observations of the 'wall-effect'. This observation also provides a basis of preferential arrangement of the cement particles within the concrete with the steel rebar and the larger aggregates behaving

as a wall thus disrupting the non-preferential arrangement of the cement particles. This results in smaller grains being closer to the 'wall' and larger grains further away.

Figure 2- BSE micrographs at 50× magnification showing coarse aggregate (CA) to be (a) typically far from the steel, and (b) a rare occurrence of a larger sized aggregate located close to the steel

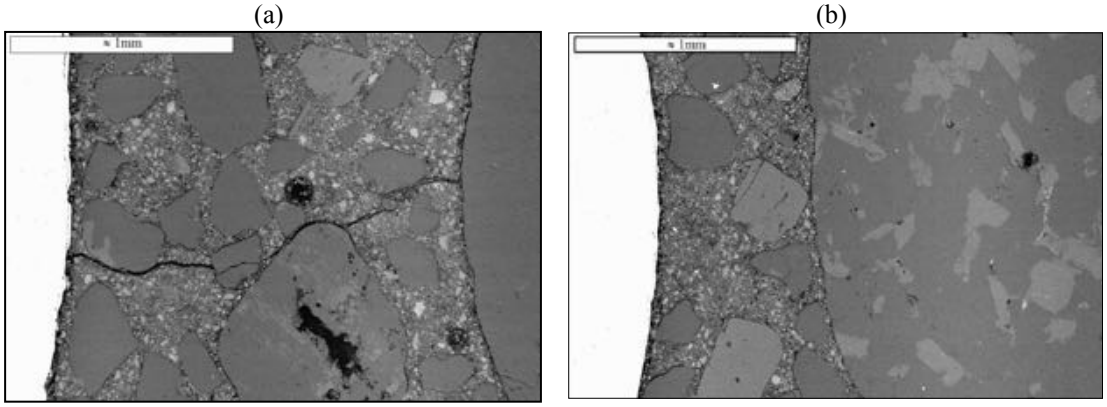

Figure 3- BSE micrograph at 50× magnification of coarse aggregate (CA) to be typically far from other CA

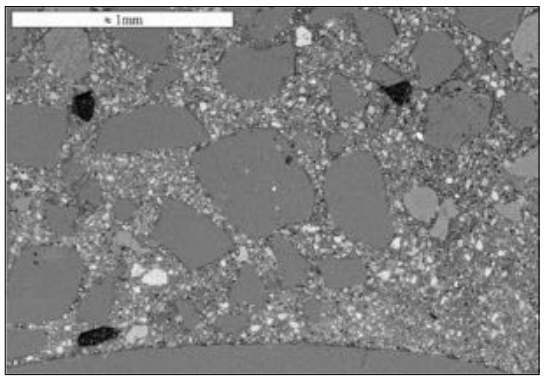

Rebars in horizontal orientation predominantly displayed underside bleeding which created a gap that remained with time. **Figure 4** shows a reinforced concrete specimen at 270 day age in horizontal orientation and the underside gap due to the bleeding effect. The bleeding effect was similarly reported in qualitative [15, 25] and quantitative [7] microstructural studies of reinforced concrete.

Figure 4- Schematic representation of bleeding occurring in a horizontal steel rebar of a 270

day old reinforced concrete specimen at 50× magnification

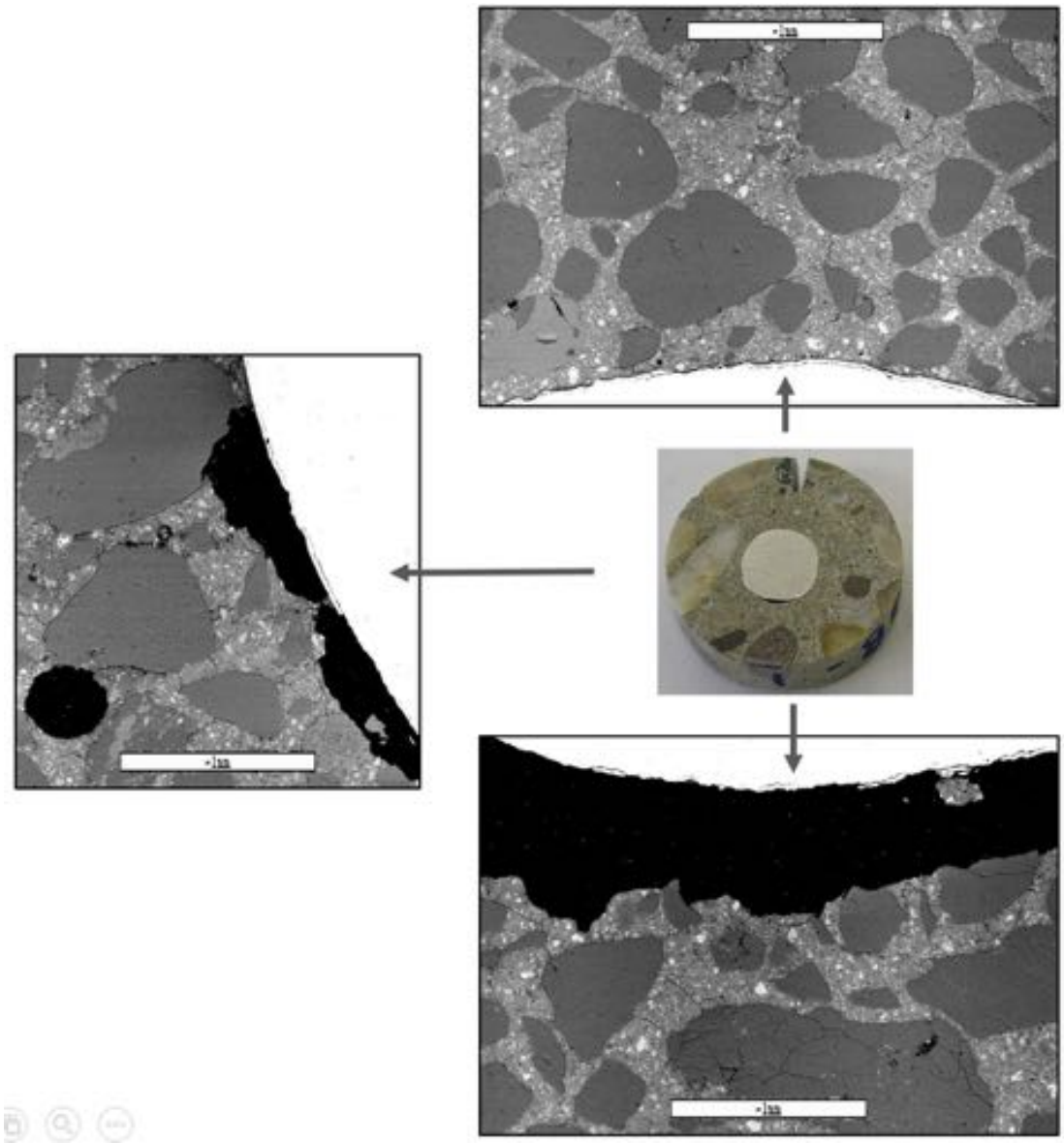

As shown in **Figure 5**, the unreacted slag particles were regularly observed to be closer to the steel interface whereas the anhydrous cement particles were further away from the steel interface. As expected, this was more obvious during the early ages where both the unreacted slag and anhydrous cement particles were prominent throughout the hardened cement paste. This finding will be discussed further in the quantitative results.

Figure 5- BSE micrograph at 500x magnification of 50% GGBS incorporated reinforced concrete at 3 day age

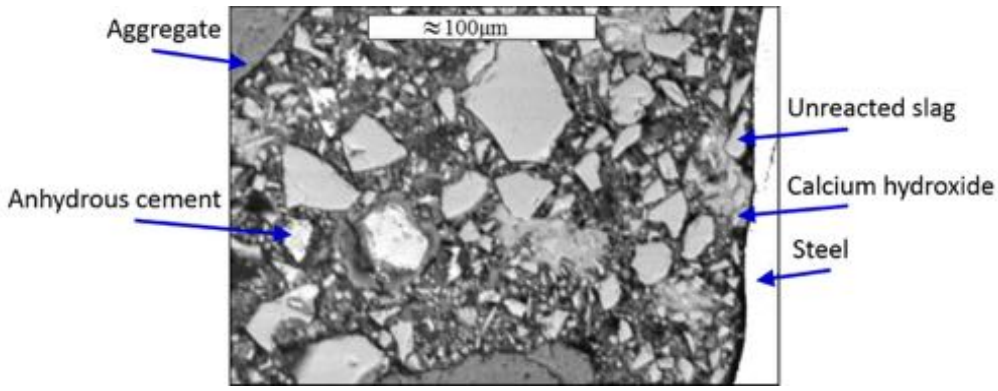

3.2. Quantitative Results of OPC Mix at 20°C

The distribution profiles of hydration products at various ages for the OPC Mix are shown in **Figure 6** for the steel-cement interface and in **Figure 7** for the aggregate-cement interface. The hydration products in both cases comprise of *(a)* Calcium Hydroxide, CH; *(b)* Porosity; *(c)* Anhydrous cement particles and *(d)* Undesignated hydration products (UHP). Porosity refers to pores with width greater than about 0.5 μm and UHP is predominantly C-S-H gel, with minor inclusions and/or intermixing of of CH, monosulphates, ettringite and pores which are too fine to be distinguished at the magnification level used. Porosity and UHP are henceforth referred as such.

Figure 6- Distribution of hydration products from the steel interface at various ages for the OPC Mix cured at 20°C
(a) Calcium Hydroxide, CH
(b) Porosity
(c) Anhydrous Cement
(d) Undesignated Hydration Products, UHP

(a)

Figure 7- Distribution of hydration products from the aggregate interface at various ages for the OPC Mix cured at 20°C
(a) Calcium Hydroxide, CH
(b) Porosity
(c) Anhydrous Cement
(d) Undesignated Hydration Products, UHP

(a)

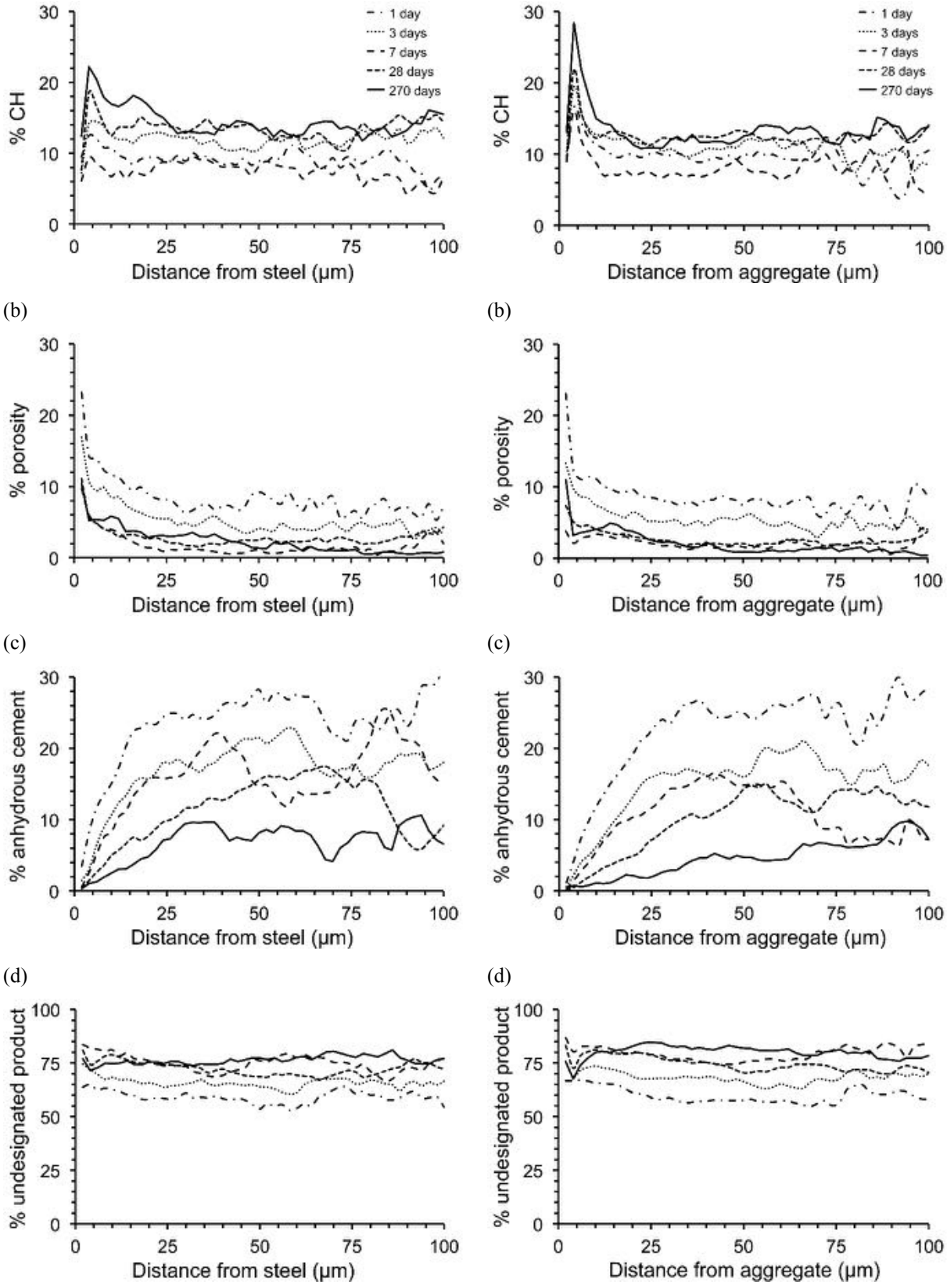

306

307 The general trend with increasing age was an increase in CH, a decrease in porosity (i.e. pores greater

308 than about 5μm), and a decrease in anhydrous cement at both the interfaces and bulk cement paste.

There was also generally an increase in UHP. The general comparison of hydration products at the interfaces with the bulk cement paste was higher CH, higher porosity and lower anhydrous cement. There was no specific trend for the UHP between the interfaces and the bulk cement paste.

The trends for the CH, porosity, anhydrous cement and UHP at each age and the subsequent changes with progressing age can be attributed to the ongoing hydration process of the cement. The differences in magnitude of the CH, porosity and anhydrous cement between both the steel- and aggregate-cement interfaces with the bulk cement paste can be attributed to the wall-effect. The generally accepted concept [21] is that during the concrete placing and compaction stages, the rebar and aggregate interfaces act as walls which disturbs the packing and arrangement of the cement grains. Under normal conditions the cement grains should have no preference in arrangement, but in the presence of these walls, the tendency would be for smaller grains to occupy the wall and larger grains further out. The increased CH at the aggregate-cement interface was similarly observed [7, 10, 24, 26-28] in other quantitative BSE microstructural studies of concrete via image analysis. In this case, the peak value close to the interface increases from about 16% at 1 day to 28% at 270 days, whilst the value in the bulk cement paste is about 14% at 270 days.

The higher quantity of CH at the steel-cement interface agrees with a number of qualitative studies of steel-concrete interfaces using fractured surfaces [2-4, 29-33] which additionally suggest that those qualitative observations may be representative of the concrete systems. Few BSE microstructural quantitative analyses have been done on the interfaces of reinforced concrete, primarily due to difficulty of specimen preparation, as discussed previously. The CH trends observed agree with the quantitative analyses reported by Horne et al. [7]. The differences in numerical values can possibly be attributed to different mixing methodologies and rebar confinements.

334 The anhydrous cement profiles showed the largest variation of results between the different ages
335 and provide the most direct comparison with the macro-structure properties of the concrete, in this
336 case the compressive strength. Whilst there was variability at greater distances from the interfaces
337 (due to poor statistics, as explained earlier), nevertheless the anhydrous content of the bulk cement
338 paste for both interfaces can be approximated to 26, 18, 16, 14 and 8% at ages 1, 3, 7, 28 and 270
339 days respectively. These results correlate well with the compressive strengths of the OPC Mix at the
340 same ages (i.e. approximately 15, 30, 44, 60 and 77 MPa from **Table 2**). For the porosity, only the 1
341 day age and 3 day age showed differences in magnitudes between the interfaces and the bulk
342 cement paste. The porosity profiles were progressively decreasing with age; the 7 day, 28 day and
343 270 day ages were approximately similar in profiles and magnitude with approximately 2% in the
344 bulk cement paste.
345
346
347 **3.3. Quantitative Results of GGBS Mixes at 20°C**
348 **Figure 8** and **Figure 9** shows the distribution profiles of hydration products at various ages for the
349 50GGBS Mix at distance away from the steel-cement and aggregate-cement interfaces respectively.
350 The hydration products comprise of *(a)* Calcium Hydroxide, CH; *(b)* Porosity; *(c)* Anhydrous cement
351 particles; *(d)* Unreacted slag and *(d)* Undesignated hydration products (UHP). Designations for
352 porosity and UHP are as per explained in Section 3.2 and are henceforth referred as such. Similarly
353 **Figure 10** and **Figure 11** shows the distribution of hydration products for the 70GGBS Mix.
354
355

Figure 8- Distribution of hydration products from the steel interface at various ages for the 50GGBS Mix cured at 20°C
(a) Calcium Hydroxide, CH
(b) Porosity
(c) Anhydrous Cement
(d) Unreacted Slag

Figure 9- Distribution of hydration products from the aggregate interface at various ages for the 50GGBS Mix cured at 20°C
(a) Calcium Hydroxide, CH
(b) Porosity
(c) Anhydrous Cement
(d) Unreacted Slag

(e) Undesignated Hydration Products

(e) Undesignated Hydration Products

356

(a)

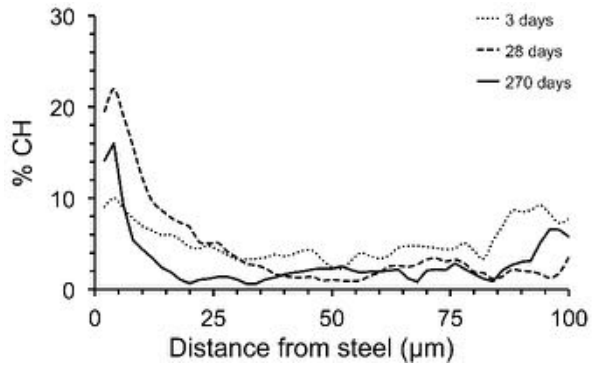

(a)

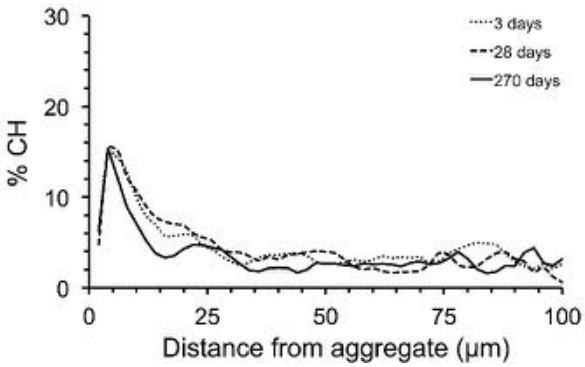

(b)

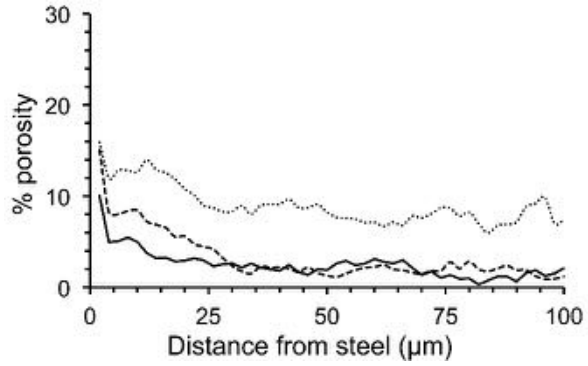

(b)

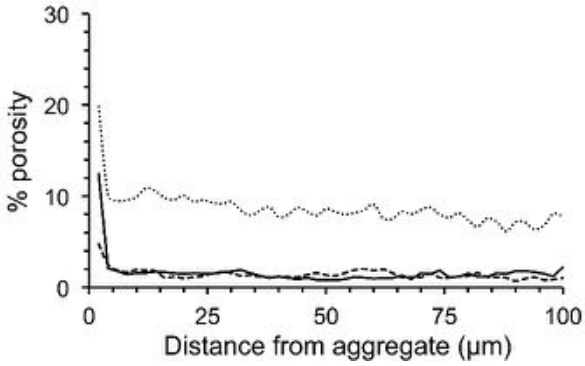

(c)

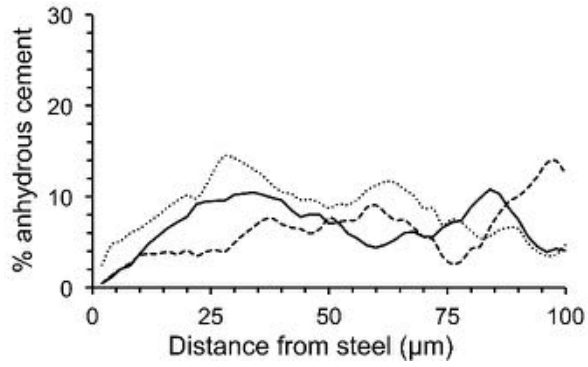

(c)

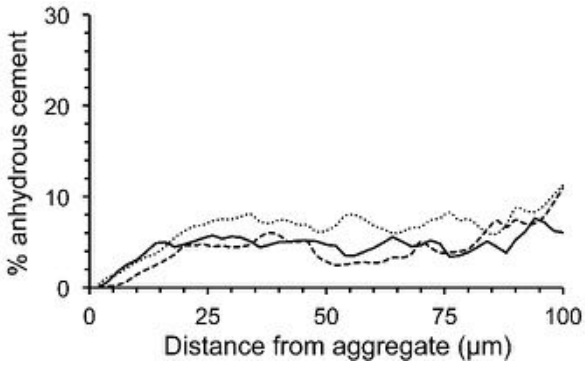

(d)

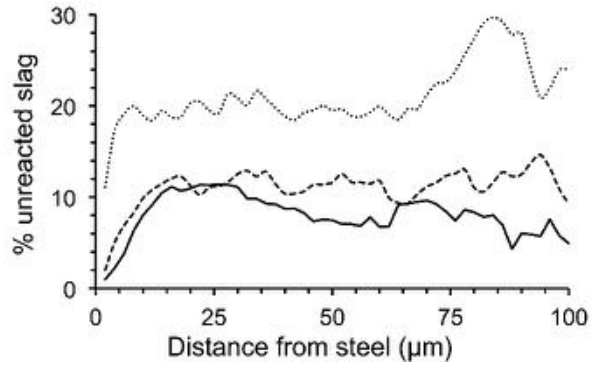

(d)

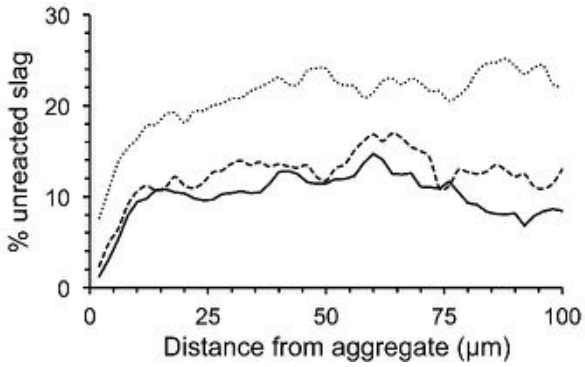

(e)

(e)

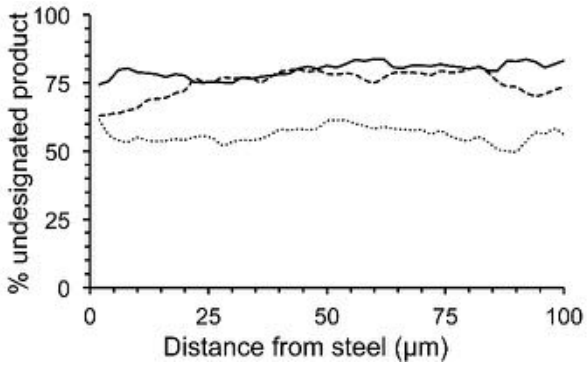

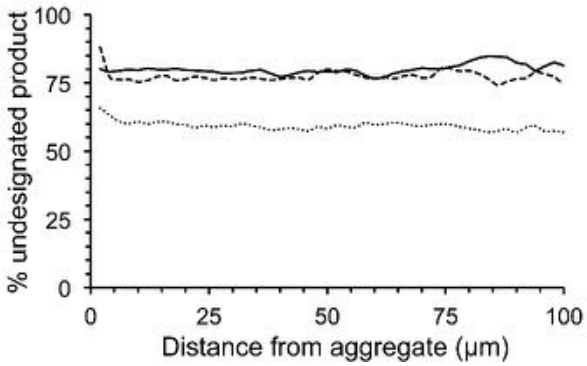

357

358

Figure 10- Distribution of hydration products from the steel interface at various ages for the 70GGBS Mix cured at 20°C

(a) Calcium Hydroxide, CH

(b) Porosity

(c) Anhydrous Cement

(d) Unreacted Slag

(e) Undesignated Hydration Products

Figure 11- Distribution of hydration products from the aggregate interface at various ages for the 70GGBS Mix cured at 20°C

(a) Calcium Hydroxide, CH

(b) Porosity

(c) Anhydrous Cement

(d) Unreacted Slag

(e) Undesignated Hydration Products

359

(a)

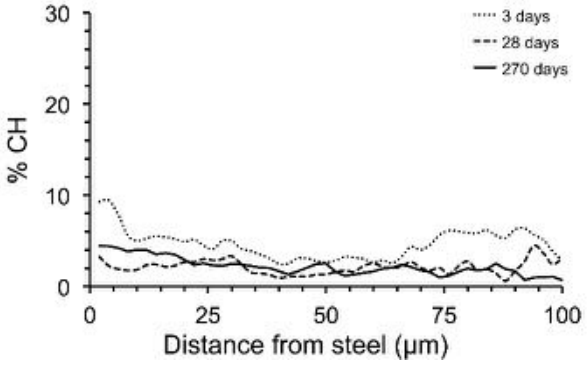

(b)

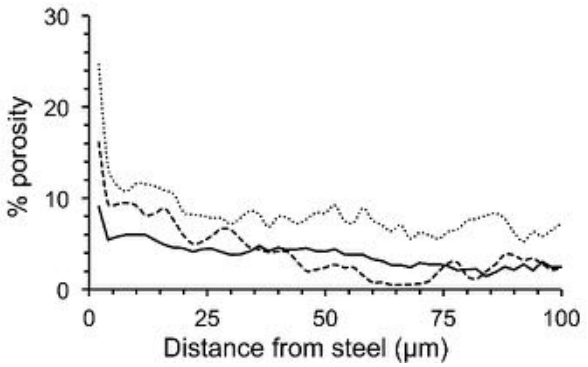

(c)

(a)

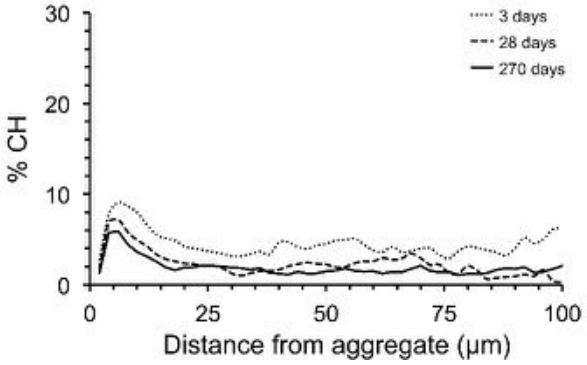

(b)

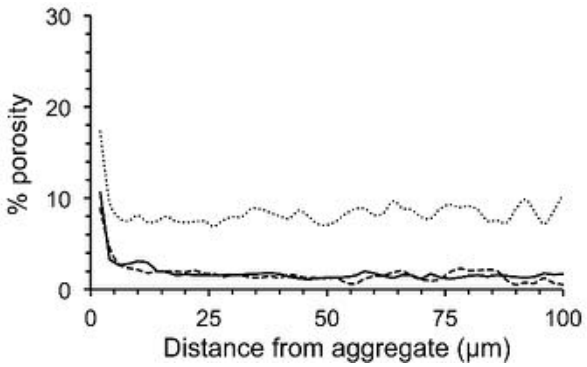

(c)

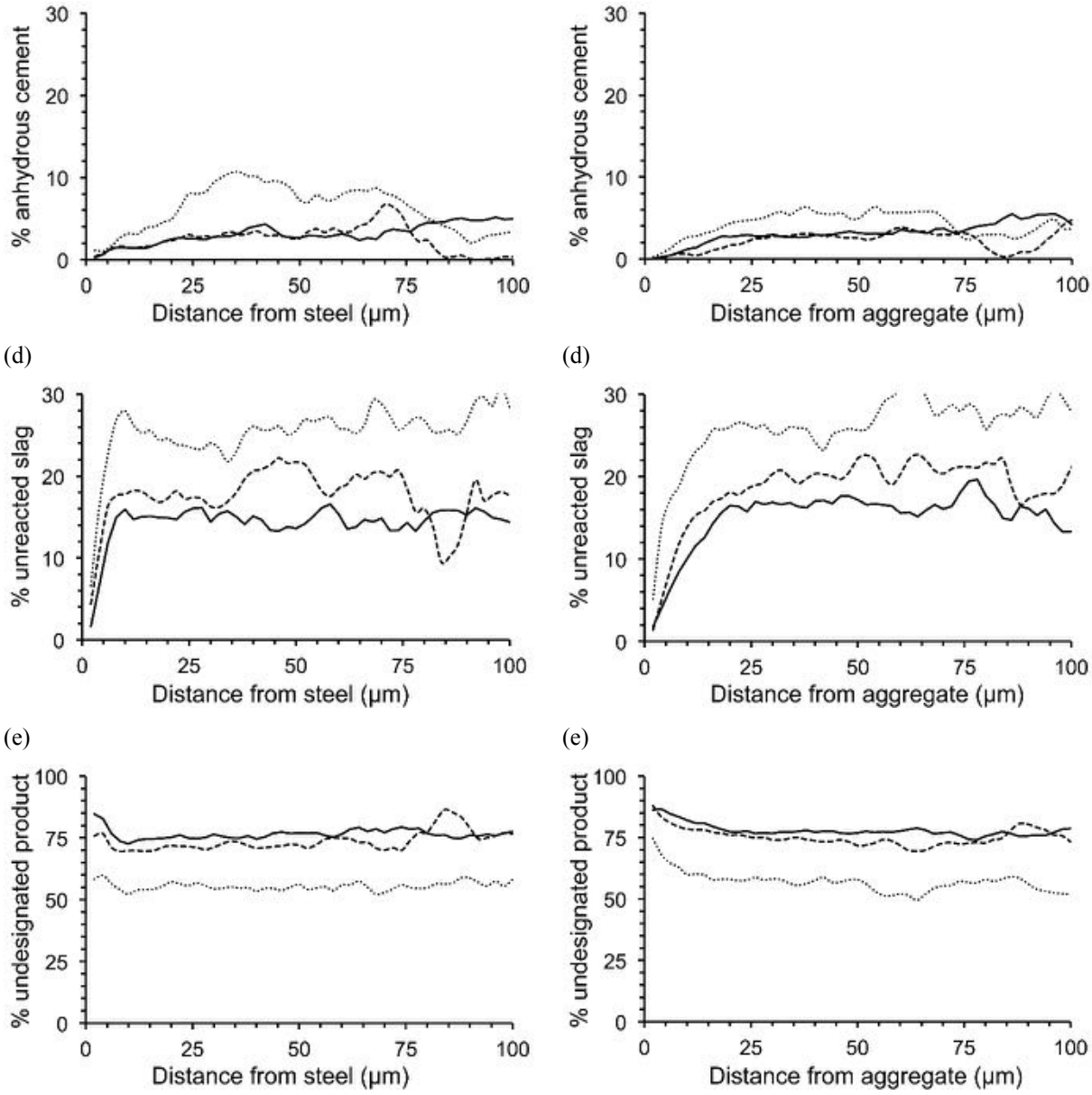

360

361

362 The general trend with increasing age for both the 50GGBBS Mix and 70GGBS Mix was a decrease in
363 porosity (i.e. pores greater than about 5μm), a decrease in unreacted slag, and an increase of UHP at
364 both the interfaces and bulk cement paste. The anhydrous cement was generally low throughout
365 although the profile at 3 day age was marginally higher compared to later ages; this was more
366 noticeable in the 70GGBS Mix. Aside from at the interfaces, the CH profiles were also generally low
367 throughout. The amount of unreacted slag was greater than anhydrous cement at each
368 corresponding age; this was especially evident with the 70GGBS Mix. The general comparison of

hydration products at the interfaces with the bulk cement paste was higher CH, higher porosity, lower anhydrous cement, and lower unreacted slag. The slope gradients of the anhydrous cement and the unreacted slag from the interfaces to the bulk cement paste differed; with the unreacted slag having a steeper gradient than the anhydrous cement profile.

A comparison between the 50GGBS Mix and the 70GGBS Mix showed the CH profiles in the bulk cement paste to be similar being low throughout all ages. Both mixes showed greater amounts of CH at the interfaces compared to the bulk cement paste; the CH profile at the interface was greater for the 50GGBS Mix. The porosity comparison showed similar profiles and levels at each corresponding age. The unreacted slag was greater in the 70GGBS Mix throughout all ages. In addition, the slope gradient of the unreacted slag at the steel-cement interface in the 70GGBS Mix was steeper than the corresponding gradient of the 50GGBS Mix, whilst was similar at the aggregate-cement interface.

The trends for the porosity, unreacted slag and UHP at each age and the subsequent change with progressing age can similarly be attributed to the ongoing hydration of both the anhydrous cement and slag particles. Similar to the OPC Mix, the differences in magnitudes of the CH, porosity, anhydrous cement and unreacted slag can also be attributed to the wall effect.

The CH profile was consistently low in the bulk cement paste throughout the ages, at approximately 2-6% ranges. This is likely due to the on-going production of CH from the hydration of the calcium silicates within anhydrous cement, which is subsequently consumed by the slag reaction to produce C-S-H. Once CH is produced and the subsequent slag reaction process initiated, would result in both reaction processes occurring simultaneously until either the reaction of anhydrous cement or slag has ceased. The interfaces showed higher CH levels compared with the bulk cement paste, however showed no specific trend with respect to age. It is likely that localised effects of either presence or absence of CH and slag had contributed to this result.

The greater volume of unreacted slag compared to anhydrous cement at early age are as expected, due to the delayed start of reaction of the slag prior to the production of CH from the calcium silicates. At early age, the volume of unreacted slag of the 70GGBS Mix is higher than that of the 50GGBS Mix. This is as expected due to the higher GGBS replacement level. The unreacted slag profile at the interfaces showed a steeper gradient than the anhydrous cement at the same age; this was especially evident at early age of 3 days. This observation suggests that there is better packing of the slag as compared to the cement, leading to a narrower ITZ. This proposal is further reinforced with the unreacted slag profile at the steel-concrete interface slope gradient being steeper for the 70GGBS Mix than the corresponding gradient in the 50GGBS mix. These findings were also observed visually from the BSE micrographs as was explained previously. Based on qualitative microstructural observations on fractured surfaces, Gao et al. [34] reported that the ITZ appeared denser with increasing GGBS content (they used 20% and 60% replacement levels) and is therefore in agreement with the findings discussed.

3.4. Comparisons Between OPC and GGBS Mixes

The profiles for the unreacted cement were generally lower for the GGBS mixes compared to the OPC Mix at each age and were as expected in consideration of the replacement. At 270 days age the quantity in the bulk paste was approximately 8, 5 and 3% for the OPC Mix, 50GGBS Mix and 70GGBS Mix respectively. It is likely that for the 70GGBS Mix both the low anhydrous cement and low CH content led to slower reaction of the slag at this late age.

The OPC Mix and GGBS mixes showed generally decreasing porosity with respect to age. The porosity profiles were similar at later ages, all showing a low level of pores > ≈0.5 μm at later ages, with similar values, except for the 70GGBS Mix which was slightly higher at approximately 4%.

However, differences were observed at early age: for example, the porosity for the GGBS mixes at 3 days was similar to that of the OPC Mix at 1 day age, which can be attributed to the slower initial hydration reaction of the slag.

The CH profiles showed steady increases both at the interfaces and in the bulk cement paste with increasing age for the OPC Mix but was not the case for the GGBS mixes. The OPC Mix followed a steady trend of increase of CH with respect to age whilst the GGBS mixes were generally low throughout, the latter likely due to the ongoing production of CH from the hydration of the calcium silicates and consumption from the slag reaction to produce C-S-H, as had been explained previously.

The OPC Mix showed a steady increase of CH at the interfaces with increasing age, which would be advantageous in terms of protection of the steel rebar from generalized corrosion due to an enhanced pH buffering capacity. The GGBS mixes also showed CH at the interface, though less than the OPC Mix at the same ages, and with no specific trend with respect to age. The approximate values of % CH present at an interface (the peak value) and in the bulk cement paste at 270 days are summarized in **Table 3**, taking into account the profiles from both the steel- and aggregate-cement paste interfaces. The lower % CH in the GGBS mixes was compensated by higher UHP, which comprises predominantly of C-S-H. Whilst providing reduced buffering capacity, it is possible that this subsequent replacement of CH at the steel interface with C-S-H might enhance protection of the steel from corrosion by providing a physical barrier to the ingress of aggressive ions.

Table 3- The approximate peak and bulk %CH after 270 days hydration and the estimated approximate thickness of the ITZ (μm)

	Approximate % CH		Estimated Thickness of the ITZ (μm)				
	Interface (Peak)	Bulk	Calcium Hydroxide	Porosity (>≈0.5 μm)	Anhydrous Cement	Unreacted Slag	UHP
OPC Mix	22-28	14	10-15	7	15-50	-	10
50GGBS Mix	16	2-4	15	5	15-20	15	0-10

70GGBS Mix	6	2	15	5	20-30	10-15	0-10

The OPC Mix and GGBS mixes showed a steady increase of % UHP, though the rates were not similar, with respect to age. Most of the differences can be attributed to the partial replacement of OPC with GGBS for the GGBS mixes and thus the initial slower reaction as compared to a neat OPC mix. The UHP profiles were inversely similar with the porosity profile relationship between the OPC Mix and GGBS mixes. At early age, the values for the % UHP in the 50GGBS and 70GGBS mixes were lower than the OPC Mix (approximately 58 and 56 % respectively, compared to 68 % at 3 days age), most likely due to the slower initial hydration of the slag. At later ages however, the values were very similar (approximately 80 and 78 % compared to 79 % at 270 days age). Since the UHP is comprised largely of C-S-H, it is perhaps unsurprising that the values for % UHP correlate quite well with the compressive strengths; the strengths of the OPC, 50GGBS, and 70GGBS mixes were approximately 30, 20 and 11 MPa at 3 days age, and 77, 80 and 67 MPa at 270 days age.

Scrivener et al. [24] considered that the effective thickness of the ITZ varies with the microstructural feature being studied and during the course of hydration. Values for the approximate width of the ITZ for the concrete samples studied in the present work are given in **Table 3**, estimated from the profiles from both steel- and aggregate-cement paste interfaces of CH, porosity, anhydrous cement and unreacted slag. It is evident that the results are consistent with Scrivener et al.'s view.

4. Conclusions

Quantitative analysis using the image analysis process was utilised for sets of BSE micrographs of OPC and OPC/GGBS reinforced concrete systems at various ages. The profiles and properties of these systems at the steel- and aggregate-cement paste interfaces and the bulk cement paste were studied. The main findings are as follows:

1. The OPC Mix generally showed increasing CH, decreasing porosity (i.e. pores greater than about 5μm), decreasing anhydrous cement and increasing UHP levels with respect to age.
2. The OPC Mix generally showed higher CH, higher porosity and lower anhydrous cement levels at the interfaces compared to the bulk cement paste.
3. The GGBS mixes generally showed decreasing porosity, decreasing anhydrous cement, decreasing unreacted slag and increasing UHP levels with respect to age. The CH was predominantly low throughout.
4. The GGBS mixes generally showed no specific trend of CH at the interfaces with respect to age. There was generally lower CH with increasing GGBS proportion.
5. The GGBS mixes generally showed higher CH, higher porosity, lower anhydrous cement and lower unreacted slag levels at the interfaces compared to the bulk cement paste.
6. The GGBS mixes generally showed lower CH, higher porosity, lower anhydrous cement and lower UHP levels at the same corresponding early age; and lower CH, similar porosity, lower anhydrous cement, and similar UHP levels at the same corresponding later ages when compared to the OPC Mix.
7. The GGBS mixes generally showed that the unreacted slag profiles had a steeper slope at the ITZ than the anhydrous cement profiles at the same age, suggesting a narrower ITZ for the GGBS mixes compared to the OPC Mix.
8. An increase in GGBS proportion led to a steeper slope of the unreacted slag profile at the ITZ, suggesting the ITZ distance is inversely proportional to the GGBS replacement level.

Acknowledgements

This work was supported by the In-service Training Scheme, Brunei Darussalam.

495

496 **References**

497 1. Corrosion Costs and Preventive Strategies in the US, Publication No. FHWA-RD-01-156, NACE,
498 https://www.nace.org/uploadedFiles/Publications/ccsupp.pdf, Last accessed: 12.11.2016.
499 2. **Page, C. L.** (1975). "Mechanism of Corrosion Protection in Reinforced Concrete Marine
500 Structures." Nature **258**(5535): 514-515.
501 3. **Pinchin, D. J. & Tabor, D.** (1978). "Interfacial phenomena in steel fibre reinforced cement II: Pull-
502 out behaviour of steel wires." Cement and Concrete Research **8**(2): 139-150.
503 4. **Al Khalaf, M. N. & Page, C. L.** (1979). "Steel/mortar interfaces: Microstructural features and
504 mode of failure." Cement and Concrete Research **9**(2): 197-207.
505 5. **Glass, G. K., R. Yang, R., Dickhaus, T., & Buenfeld, N. R.** (2001). "Backscattered electron imaging
506 of the steel-concrete interface." Corrosion Science **43**(4): 605-610.
507 6. **Zayed, A. M.** (1992). "The Nature of the Concrete-Steel Rebar Interface in Plain and Silica Fume
508 Concrete." Materials Research Society: Symposium Proceedings, Materials Research Society.
509 7. **Horne, A. T., Richardson, I. G., & Brydson, R. M. D.** (2007). "Quantitative Analysis of the
510 Microstructure of Interfaces in Steel Reinforced Concrete." Cement and Concrete Research **37**:
511 1613-1623.
512 8. **Kenny, A., & Katz, A.** (2012). "Characterization of the interfacial transition zone around steel
513 rebar by means of the mean shift method." Materials and Structures, **45**(5), 639-652.
514 9. **Kenny, A., & Katz, A.** (2015). "Statistical relationship between mix properties and the interfacial
515 transition zone around embedded rebar." Cement and Concrete Composites, **60**, 82-91.
516 10. **Scrivener, K. L.** (1999). Characterisation of the ITZ and its Quantification by the Test Methods.
517 Engineering and Transport Properties of the Interfacial Transition Zone in Cementitous
518 Composites. M. G. Alexander, G. Arliguie, G. Ballivy, A. Bentur and J. Marchand, RILEM**:** 3-15.

11. **Wainwright, P. J., Cabrera, J. G., & Alamri, A. M.** (1992). Performance Properties of Pozzolanic Mortars Cured in Hot Dry Environments. Concrete in Hot Climates: Proceedings of the Third International RILEM Conference, E & FN Spon.
12. **Güneyisi, E., Özturan, T., & Gesoğlu, M.** (2005). "A Study on Reinforcement Corrosion and Related Properties of Plain and Blended Cement Concretes Under Different Curing Conditions." Cement and Concrete Composites **27**: pp.449-461.
13. **Cheng, A., Huang, R., Wu, J. K., & Chen, C. H.** (2005). "Influence of GGBS on durability and corrosion behavior of reinforced concrete." Materials Chemistry and Physics **93**(2-3): 404-411.
14. **Pal, S. C., Mukherjee, A., & Pathak, S. R.** (2002). "Corrosion behavior of reinforcement in slag concrete." ACI Materials Journal **99**(6): 521-527.
15. **Mohammed, T. U., Yamaji, T., & Hamada, H.** (2002). "Microstructures and interfaces in concrete after 15 years of exposure in tidal environment." ACI Materials Journal **99**(4): 352-360.
16. **Richardson, I. G. & Groves, G. W.** (1992). "Microstructure and Microanalysis of Hardened Portland Cement Pastes Involving Ground Granulated Blast-Furnace Slag." Journal of Material Science **27**: 6204-6212.
17. **Taylor, R., Richardson, I. G., & Brydson, R. M. D.** (2010) "Composition and microstructure of 20-year-old ordinary Portland cement–ground granulated blast-furnace slag blends containing 0 to 100% slag." Cement and Concrete Research **40:** 971-983.
18. **Brough, A. R. & Atkinson, A (2000)**. "Automated identification of the aggregate-paste interfacial transition zone in mortars of silica sand with Portland or alkali-activated slag cement paste." Cement and Concrete Research **30**(6): 849-854.
19. **Angst, U.M., Geiker, M.R., Michel, A. et al.** (2017). "The steel–concrete interface." Materials and Structures 50:143. https://doi.org/10.1617/s11527-017-1010-1
20. **Richardson, I. G.** (2002). Electron Microscopy of Cements. Structure and Performance of Cements. J. Bensted and P. Barnes (Eds), Spon Press. 500-566.

21. **Scrivener, K. L.** (2004). "Backscattered Electron Imaging of Cementitious Microstructures: Understanding and Quantification." Cement and Concrete Composites **26**(8): 935-945.
22. **Duraman, P. S. B. P.** (2007). Microstructure & Properties of Steel-Reinforced Concrete Systems Hydrated at 20C and 38C. School of Civil Engineering. Leeds, University of Leeds. **PhD Thesis**.
23. **Bentur, A. & Odler, I** (1996). Development and Nature of Interfacial Microstructure. Interfacial Transition Zone in Concrete. J. C. Maso, E&FN Spon**:** 18-44.
24. **Scrivener, K. L., Crumbie, A. K., & Laugesen, P.** (2004). "The Interfacial Transition Zone (ITZ) Between Cement Paste and Aggregate in Concrete." Interface Science **12**: 411-421.
25. **Soylev, T. A. & Francois, R.** (2003). "Quality of steel-concrete interface and corrosion of reinforcing steel." Cement and Concrete Research **33**(9): 1407-1415.
26. **Wang, Y. & Diamond, S.** (1995). "An Approach to Quantitative Image Analysis for Cement Pastes." Materials Research Society: Symposium Proceedings, Materials Research Society.
27. **Diamond, S. & Huang, R** (1998). The Interfacial Transition Zone: Reality or Myth? The Interfacial Transition Zone in Cementitious Composites. A. Katz, A. Bentur, M. Alexander and G. Arliguie, E&FN Spon**:** 1-39.
28. **Head, M. K.** (2001). Influence of the Interfacial Transition Zone (ITZ) on the Properties of Concrete. School of Engineering. Leeds, University of Leeds. **PhD Thesis**.
29. **Monteiro, P. J. M., Gjorv, O. E., & Mehta, P. K.** (1985). "Microstructure of the steel-cement paste interface in the presence of chloride." Cement and Concrete Research **15**(5): 781-784.
30. **Glasser, F. P. & K. K. Sagoe-Crenstil** (1989). "Steel in Concrete: Part II Electron Microscopy Analysis." Magazine of Concrete Research **41**(149)**:** 213-220.
31. **Leek, D. S. & Poole, A. B.** (1990). The Breakdown of the Passive Film on High Yield Mild Steel by Chloride Ions. Corrosion of Reinforcement in Concrete, C. L. Page, K. W. J. Treadway and P. B. Bamforth, Elsevier: 65-73.

32. **Gallias, J. L.** (1998). Microstructure of the Interfacial Transition Zone Around Corroded Reinforcement. The Interfacial Transition Zone in Cementitous Composites. A. Katz, A. Bentur, M. Alexander and G. Arliguie, E&FN Spon**:** 171-178.

33. **Yue, L. & Shuguang, H.** (2001). "The microstructure of the interfacial transition zone between steel and cement paste." Cement and Concrete Research **31**(3): 385-388.

34. **Gao, J. M., Qian, C. X., Liu, H. F., Wang, B., & Li, L.** (2005). "ITZ microstructure of concrete containing GGBS." Cement and Concrete Research **35**(7): 1299-1304.